Joint interpretation of AEM and aeromagnetic data acquired over the Drybones kimberlite, NWT (Canada)

Domenico Di Massa [a,*], Maurizio Fedi [b], Giovanni Florio [b], Andrea Vitale [b], Andrea Viezzoli [c], Vlad Kaminski [c]

[a] Geophysical Consultant at DIMMS CONTROL Srl, Italy
[b] Univerity of Naples Federico II, Italy
[c] Aarhus Geophysics Aps, Denmark

ARTICLE INFO

ABSTRACT

We present the joint interpretation of airborne electromagnetic and aeromagnetic data, acquired to study kimberlite pipes. We analyse the data surveyed in 2005 over Drybones Bay, Archean Slave Province of the Northwest Territories, northern Canada. This area hosts a recently discovered kimberlite province with >150 kimberlite pipes.

Magnetic and electromagnetic data were each one modelled by 1D inversion. For magnetic data we inverted vertical soundings built through upward continuations of the measured data at various altitudes. The validity of the method was prior verified by tests on synthetic data. Electromagnetic data were processed and inverted using the modified AarhusINV code, with Cole-Cole modelling, in order to take into account induced polarization effects, consisting in negative voltages and otherwise skewed transients.

The integrated study of the two kinds of data has led to a better understanding of the structures at depth, even though the comparison between the magnetic and the electromagnetic models shows the different sensitivity of the two methods with respect to the geological structure at Drybones Bay.

1. Introduction

Time domain electromagnetic (TDEM) and magnetic surveys are often performed simultaneously, by a single airborne system carrying both the electromagnetic equipment and the magnetic sensor.

The opportunity of having two distinct datasets over the same area, obeying to different physical principles and thus reflecting the distribution of different physical properties within the Earth is, in principle, of great value. In fact, it makes possible an integrated study of the two types of data with a potentially strong improvement of the final interpretation model.

In this paper, we focused on modelling airborne electromagnetic (AEM) and aeromagnetic data acquired during the same survey in Canada, at Drybones Bay in the Archean Slave Province of the Northwest Territories, northern Canada. In this area, in 1994, a completely underwater kimberlite structure was discovered.

The application of geophysical methods to exploration for kimberlites and their associated diamonds began over 50 years ago with the use of magnetic and gravity measurements. Within a decade, electrical resistivity and, later, induced polarization methods were also applied

to the same case. Since 1970's, both ground and airborne methods included magnetic and electromagnetic measurements (Reed and Witherly, 2007).

Kimberlite is an alkali ultramafic igneous rock, formed from the cooling of molten magma that arises from the melt of peridotite in the mantle at depth of 150–200 km. Kimberlite is composed of at least 35% olivine, together with other minerals such as mica, serpentine, and calcite (Kjaarsgard, 1996). During its upward rise into the upper mantle and overlying crust, minerals start to crystallize while the volatile gases expand and exert increasingly higher pressures on the surrounding rocks, eventually breaking some of the surrounding rock and incorporating it into the magma. The kimberlite magma may produce explosive volcanic events. In the Slave Craton and adjacent areas, these eruptions occurred from subaerial to shallow subaqueous environments; consequently, many of the resulting vent systems are vertical or steeply dipping carrot-shaped bodies, equidimensional in a plan section and tapering gradually with depth. Kimberlite intrusions tend to occur in clusters or fields, with the large-scale distribution possibly controlled by deep-seated structural features and local emplacement controlled by shallow zones of weakness, such as faults or the margins of diabase dykes (Power and Hildes, 2007).

The accepted pipe model includes three different zones from top to bottom, each with distinctive morphology and texture: the crater, diatreme and hypabyssal zones (Scott Smith, 1996).

---

* Corresponding author.
E-mail address: d.dimassa@dimms.it (D. Di Massa).

Crater kimberlites are usually basin shaped excavations formed at the surface by explosive volcanic eruptions. Crater facies kimberlites are a mixture of tuffaceous kimberlite, surrounding country rock and overlying sediments. Two main categories of rocks are found in facies of crater kimberlites: pyroclastic, deposited by eruptive forces, and epiclastic, which are the same rocks after the interaction with water. In much of the Slave Craton, crater-facies kimberlites include a significant component of shale and mudstone, sometimes with a significant component of entrained organic material. Large blocks of surrounding country rock (xenoliths) shattered from the volcanic vent margins are present in some pipes. A crater-facies kimberlite is often deeply weathered and serpentinized (Kjarsgaard, 1996).

Kimberlite diatremes are cone-shaped bodies with vertical axes and steeply inward dipping margins. Diatreme facies describe an explosive kimberlite breccia composed of fine-grained kimberlite, mantle nodules and angular fragments of the surrounding country rocks. Diatreme facies rocks are generally confined to a central breccia pipe and are generally less altered than crater facies rocks.

Hypabyssal kimberlites consist of unaltered fine-grained kimberlite with mantle nodules and rare fragments of country rock. Hypabyssal kimberlite bodies include dykes, blind intrusions and the root zones of kimberlite pipes.

In each kimberlite field, all three facies may be present at surface because of differential glacial abrasion and quarrying, and because of blind intrusions. The depth of erosion can vary over distances of a few tens of kilometres or less. Our ability to detect a kimberlite deposit by geophysical methods depends on its physical property contrasts with the host rocks. In the Slave Craton region (Canada), magnetic anomalies are commonly associated with kimberlite intrusions, having a higher magnetic susceptibility than surrounding gneisses and granites. In fact, diatreme and hypabyssal facies are readily detected. In addition, they can be affected by remanent magnetization. Instead, for crater facies, the associated magnetic anomalies can be subtle, due to the low magnetic contrast with the surrounding rocks, which in turn depends on the proportion of the non-susceptible sediments present (Power and Hildes, 2007).

In general, the electrical resistivity of kimberlites increases with depth, from crater facies through hypabyssal facies. Consequently, crater facies display the greatest contrast in electrical properties with respect to country rocks, so being well detectable with electromagnetic (EM) methods. In fact, during weathering, a highly conductive clay-rich zone forms in the top of the pipe (Macnae, 1979). Moreover, this top layer can produce a measurable induced polarization (IP) effect, which is related to ability of the material to retain electrical charges.

However, the existence of fine grained glacial-fluvial and lake sediments in the shield regions of northern Canada, with an electrical resistivity and an electrical chargeability comparable to that of the crater facies, makes the discrimination between these sources complicated. When the resistivity contrast is negligible, a potential crater facies of kimberlite target can be still identified indirectly, by assessing if the conductor persists at depth below the overburden thickness (Power and Hildes, 2007). Diatreme and hypabyssal kimberlites have usually low electrical properties contrast with respect to the country rocks. For this reason, they are almost indistinguishable from granitic or gneissic country rocks, as based on the study of the electrical resistivity or electrical chargeability distribution at depth.

In conclusion, a cooperative modelling of magnetic and electromagnetic data is expected to yield a comprehensive information on the whole kimberlite structure, improved with respect to the analysis of just one of the two datasets.

2. Inversion of magnetic data

In this paper, we performed the inversion of magnetic data along vertical profiles. This 1D method has been proposed for gravity data (Fedi and Rapolla, 1995; Vitale et al., 2016) and it is here adapted to the magnetic case, as described below. 1D methods mainly have the advantage of a low computational complexity (Auken and Christiansen, 2004; Lane et al., 2004). The inversion of electromagnetic data (next section) is, on the other hand, commonly performed with 1D models, so our common 1D approach to the inversion of the two different datasets should warrant an easy comparison between the inverted magnetic and EM models. As a matter of fact, 2D and 3D models are built by joining the results from the whole set of independent 1D inversions, resulting in an approximate 3D model.

The basic idea of the 1D algorithm for potential fields is that the physical property distribution can be deduced from the field known at different altitudes (Fedi and Rapolla, 1995). For a set of N magnetic data along a vertical direction (vertical sounding) $[P_{k1}, ..., P_{kj}, ..., P_{kN}]$, assuming that the magnetization could vary only along the vertical direction (1D assumption), the forward problem for a continuous magnetization J, linearly related to the magnetic data B, is expressed by (Blakely, 1996):

$$B(P_{kj}) = \frac{\mu_0}{4\pi} \hat{\mathbf{F}} \cdot \nabla \int_V \mathbf{J}(r) \cdot \nabla \frac{1}{|r - r_{kj}|} dv \tag{1}$$

where $\hat{\mathbf{F}}$ is the unit-vector along the inducing field direction, k is an index accounting for the horizontal position of the vertical soundings and $j = 1, ..., N$ refer to the data positions along each kth vertical sounding.

If the source volume is subdivided in M layers, where in each of them the magnetization is homogeneous, we have:

$$B(P_{kj}) = \sum_{i=1}^{M} J_i G_{ij}(P_{kj}) \tag{2}$$

where

$$G_{ij}(P_{kj}) = \frac{\mu_0}{4\pi} \hat{\mathbf{F}} \cdot \nabla \int_{V_i} \nabla \frac{1}{|r - r_{kj}|} dv \tag{3}$$

is the unit magnetization intensity contribution due to the ith prismatic layer; $[J_1, ..., J_i, ..., J_M]$ and $[V_1, ..., V_i, ..., V_M]$ are respectively the magnetizations and the volumes of the M layers.

Eq. (2) may be rewritten in vectorial notation as:

$$\mathbf{B} = \mathbf{GJ} \tag{4}$$

where $\mathbf{B}$ represents the data vector (with dimensions Nx1) of the vertical sounding, $\mathbf{J}$ represents the unknown vector (with dimension Mx1) in the source volume and $\mathbf{G}$ represents the matrix of the theoretical kernel (with dimension NxM), defined by the eq. 3.

Since the number of layers is usually greater than the data number, eq. (4) leads to solve an indeterminate linear problem.

In particular, we search the solution having the minimum Euclidean length:

$$\mathbf{J^T J} = \sum_{i=1}^{M} J_i^2 = \|\mathbf{J}\|_2^2 = minimum \tag{5}$$

which satisfies some linear inequality constraints:

$$\mathbf{B} - d\mathbf{B} \leq \mathbf{GJ} \leq \mathbf{B} + d\mathbf{B} \tag{6}$$

$$j_L \leq J_i \leq j_U, \quad i = 1, ..., M \tag{7}$$

where $d\mathbf{B}$ is the vector of the experimental data error, j_L and j_U are the lower and the upper bounds of the model parameters.

The inequality constraints are defined based on the following strategy:

1 the unknown parameters vector must satisfy the forward model, but taking into account experimental data errors $d\mathbf{B}$;
2 the unknown parameters vector is bounded to avoid unrealistic estimates based on a priori knowledge about the subsurface geology.

This is an indeterminate problem with inequality constraints, which may be posed as:

$$\mathbf{FJ} \geq \mathbf{h} \qquad\qquad 8$$

where:

$$F = \begin{bmatrix} I \\ -I \\ G \\ -G \end{bmatrix}, h = \begin{bmatrix} J_L \\ -J_U \\ B - \delta B \\ -(B + \delta B) \end{bmatrix} \qquad (9)$$

The $\mathbf{F}$ matrix, containing the identity matrix $\mathbf{I}$ (*MxM*) and the kernel $\mathbf{G}$ (*NxM*), has dimension $(2M + 2N) \times M$; the vector $\mathbf{h}$, containing the lower and the upper bounds of model parameters and the data with the experimental errors, has dimension $(2M + 2N) \times 1$.

According to Menke (1989), the problem 8 may be transformed into:

$$\mathbf{Eu} = \mathbf{f} \rightarrow \begin{bmatrix} \mathbf{F}^T \\ \mathbf{h}^T \end{bmatrix}; \mathbf{u} = \begin{bmatrix} 0 \\ 1 \end{bmatrix} \qquad (10)$$

Thus, the inversion problem reduces to find the vector $\mathbf{u}$ that minimizes:

$$\mathbf{e} = \|\mathbf{f} - \mathbf{Eu}\|_2 \ subject\ to: \mathbf{u} \geq 0 \qquad (11)$$

It can be shown (Menke, 1989) that if the prediction error, $\mathbf{e}$, is null then the constraints $\mathbf{FJ} \geq \mathbf{h}$ are inconsistent, but if $\mathbf{e} \neq 0$, constraints $\mathbf{FJ} \geq \mathbf{h}$ are consistent and the solution of the problem is:

$$J_i = -\frac{e^T_i}{e^T_{M+1}} with\ i = 1:M. \qquad (12)$$

Before applying the inversion method to real cases, we tested it on synthetic magnetic dataset.

The multilevel dataset, representing the vertical soundings, were built by first computing the magnetic response of a prismatic source on a large surface at a single height, and then at a set of altitudes by upward continuation (e.g., Baranov, 1976; Blakely, 1996) of these data.

However, the upward continuation operator introduces some errors in the calculated data. This because we approximate the continuous problem with a finite and discrete set of data, on a finite region. Following Castaldo et al. (2014), the effects of this error can be mitigated by using a third-order polynomial:

$$H(z) = c_1 + c_2 z + c_3 z^2 + c_4 z^3 \qquad (13)$$

where c_1, c_2, c_3 and c_4 are unknown coefficients that should be estimated during the inversion process.

For this test, we used a single prismatic source with horizontal dimensions equal to (250, 150) m and extending at depth from 100 m to 300 m. The magnetization contrast with the surrounding volume is 3 A/m. We considered in this case only that the magnetization is purely induced, with 60° inclination and 0° declination. The magnetic anomaly generated by this source and calculated at the ground surface is shown in Fig. 1.

The vertical soundings consist of magnetic data continued at 20 different altitudes from the first level at 5 m up to the last level at 100 m, with a 5 m constant vertical step. The horizontal positions of the vertical soundings are shown in Fig. 1 by the green points, while the magnetic anomalies along the profile and at different heights, are shown in Fig. 2.
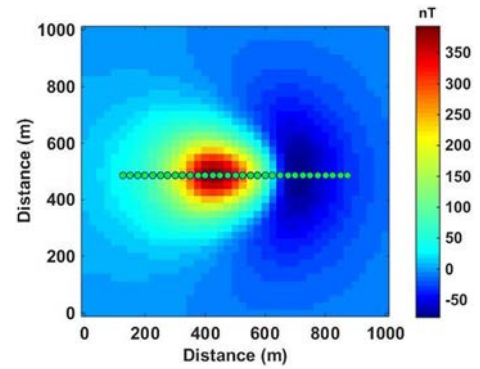

Fig. 1. Magnetic anomaly generated by a single buried prismatic source. The green dots represent the horizontal positions of the vertical soundings. (For interpretation of the references to colour in this figure legend, the reader is referred to the web version of this article.)

For the calculation of the kernel, a source volume has been defined with horizontal dimensions and the directions of the magnetization that agree with those of the true source. The vertical dimension of this volume is defined in such a way to completely contain the source of anomaly and it is discretized with 100 layers having an equal thickness of 10 m (Fig. 3).

To perform the inversion, for each vertical sounding, we computed, at its position along the selected profile, the kernel G_{ik}.

In this way, each vertical sounding is inverted independent of each other.

The procedure may be described as follows. Let us first consider a single vertical sounding, in Fig. 3. After inverting for the magnetization of the source layers, the result is then attributed to a set of layers sized as ΔX, i.e., the step size of the vertical soundings along the profile, and centred at the sounding position. Repeating this procedure for all the soundings we are finally allowed reconstructing an approximate 2D model of the source distribution along the profile.

For this test, we used the correct magnetization contrasts for the lower and the upper bounds, setting the lower bound equal to 0 and the upper bound equal to 3 A/m. The experimental error is set to a low value, equal to $5 \cdot 10^{-2}$ nT.

As shown in Fig. 4, the Vertical Soundings inversion can correctly recover the depth to the top of the source, and the magnetization contrast is properly estimated (the black rectangle in figure identifies the exact location of the buried body).

However, the model presents a gradual decreasing of the magnetization with the depth, so that an accurate estimation of the depth of the bottom is difficult.

From the model of Fig. 4, we calculated the estimated data along the profile, at a single altitude (in this case the first height, 5 m), and we
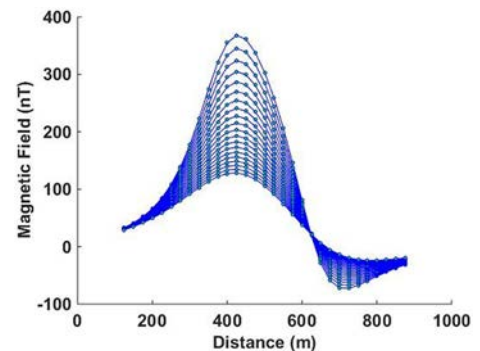

Fig. 2. Magnetic profiles at different altitudes: 5 m up to 100 m, with a 5 m constant vertical step, along the profile in Fig. 1 .
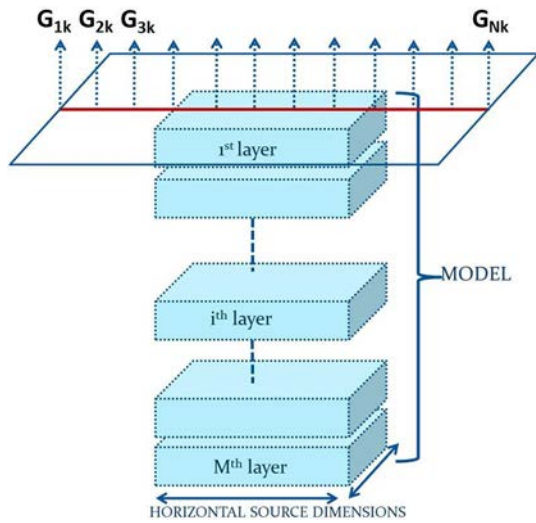
Fig. 3. Schematic picture of the finite layers forming the source volume. Dashed arrows indicate the horizontal positions of the vertical soundings. The single kernels, G_{ik} ($i = 1..$ N), are computed according to the spatial coordinates of the relative sounding.

compared them with the observed data (Fig. 5). The observed data are very well reproduced all along the profile.

The good quality of this result is noteworthy, if we consider that the 2D model is built by simply joining and interpolating the 1D inverted models obtained by independent vertical soundings.

3. VTEM survey over Drybones kimberlite

We now analyse the EM and magnetic data related to the Versatile Time Domain Electromagnetic (VTEM) survey flown in 2005 over Drybones kimberlite (Kaminski et al., 2010; Kaminski and Oldenburg, 2012).

In 1991, in the Archean Slave Province of the Northwest Territories (NWT), northern Canada, a significant new kimberlite province, hosting >150 kimberlite pipes was discovered (Kretchmar, 1995).

The Slave Province is an Archean segment of the North American Craton, composed of granites, gneisses and supracrustal rocks. Sialic basement remnants, well documented in this province, include some of the oldest rocks in the world as the Acasta gneisses in the western part of the province, which have been dated at 3.96 Ga (Bowring and Housch, 1995). Metasedimentary and metavolcanic rocks of the Yellowknife Supergroup, deposited mainly between 2.71 Ga and 2.61 Ga, are the most abundant rocks of the crustal sequences. At least five swarms of Proterozoic diabase dykes cut the older units in the central Slave Province (Le Cheminant and van Breemen, 1994; Le Cheminant et al.,
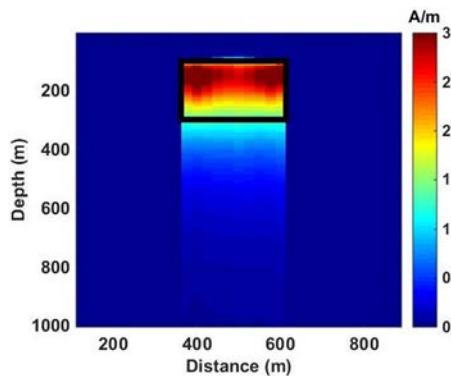

Fig. 4. Vertical Soundings inversion of the magnetic data produced by a single buried prismatic source and continued at 20 different altitudes. The black rectangle identifies the horizontal and vertical positions of the anomaly source.
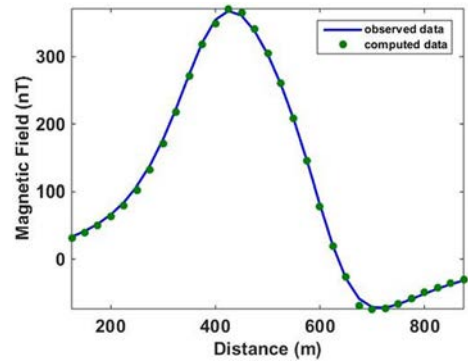

Fig. 5. Comparison between observed and computed data.

1996). The Slave Province is a classic setting for diamondiferous kimberlites: a stable Archean craton with a cool mantle root, which is necessary for the development of the diamond stability field (Haggerty, 1986; Janse, 1993). Kimberlite intrudes granites, metasedimentary rocks and, in some cases, diabase dykes. After the kimberlite emplacement, the area was covered by Laurentide ice during the Late Wisconsinan glaciation (Pell, 1995).

Middle Jurassic-, Late Ordovician-, and Cambrian-aged kimberlites have been discovered, some of which have good economic potential. Most of the kimberlites in the Slave Province do not crop out at surface; they have been identified using a combination of heavy mineral sampling, geophysical techniques and drilling. Many of the pipes are characterized by either high or low magnetic anomalies and low resistivity values.

The Drybones kimberlite is in Drybones Bay, situated approximately 45 km SE from the town of Yellowknife (NWT, Canada; Fig. 6a). The kimberlite was discovered in 1994 with a single drill hole and lies completely under the water of the Great Slave lake, at an average depth of 35–40 m; a thickness of 65–75 m of lake sediments (clay, till and sand), further covers the kimberlite (Kretchmar, 1995). The morphology of the pipe, in Fig. 6b, shows a spatially elongated intrusion (900 m by 400 m), consisting of crater, pyroclastic and diatreme facies (Kretchmar, 1995).

A geological cross-section (Fig. 6c), along the profile AA', has been drawn based on drilling information (Kretchmar, 1995).

The bedrock geology in Drybones area consists of Archean granite, granodiorite and tonalite (Kretchmar, 1995). Metasediments of Yellowknife supergroup are also present (Dunn et al., 2001). In addition, there are several known faults near the kimberlite area while a diabase dike in the northern part crosses the area from E to W (Dunn et al., 2001).

The helicopter borne geophysical survey used the VTEM system for the EM data and a caesium magnetometer for the aeromagnetic data (Witherly et al., 2004). The EM system is concentric and oriented along the vertical direction. The receiver coils were towed at a mean distance of 45 m below the aircraft. The VTEM decay was sampled using 25 time-measurement gates in the range from 0.130 to 6.340 ms after the time-off. The strength of magnetic field is measured by a magnetic sensor mounted in a separate bird, 20 m below the helicopter. The VTEM survey was carried out in 2005 along 9 flight lines spaced 100 m, on average, with orientation approximately N—S (Fig. 7). The EM data, as shown in Fig. 7, display an evident IP effect in the central part of the profiles above Drybones Bay, where the kimberlite is located. This IP effect has been identified across all flight lines, showing the existence of negative voltage data in transients.

EM data were inverted using a 1D Spatially Constrained Inversion (SCI) approach (Viezzoli et al., 2008) implemented in a modified AarhusINV code, with capability of Cole-Cole modelling (Cole and Cole, 1942; Fiandaca et al., 2012). In fact, it is common to ignore the IP effects in VTEM data by simply removing negative voltage data before the inversion. This operation can however cause a loss of resolution at
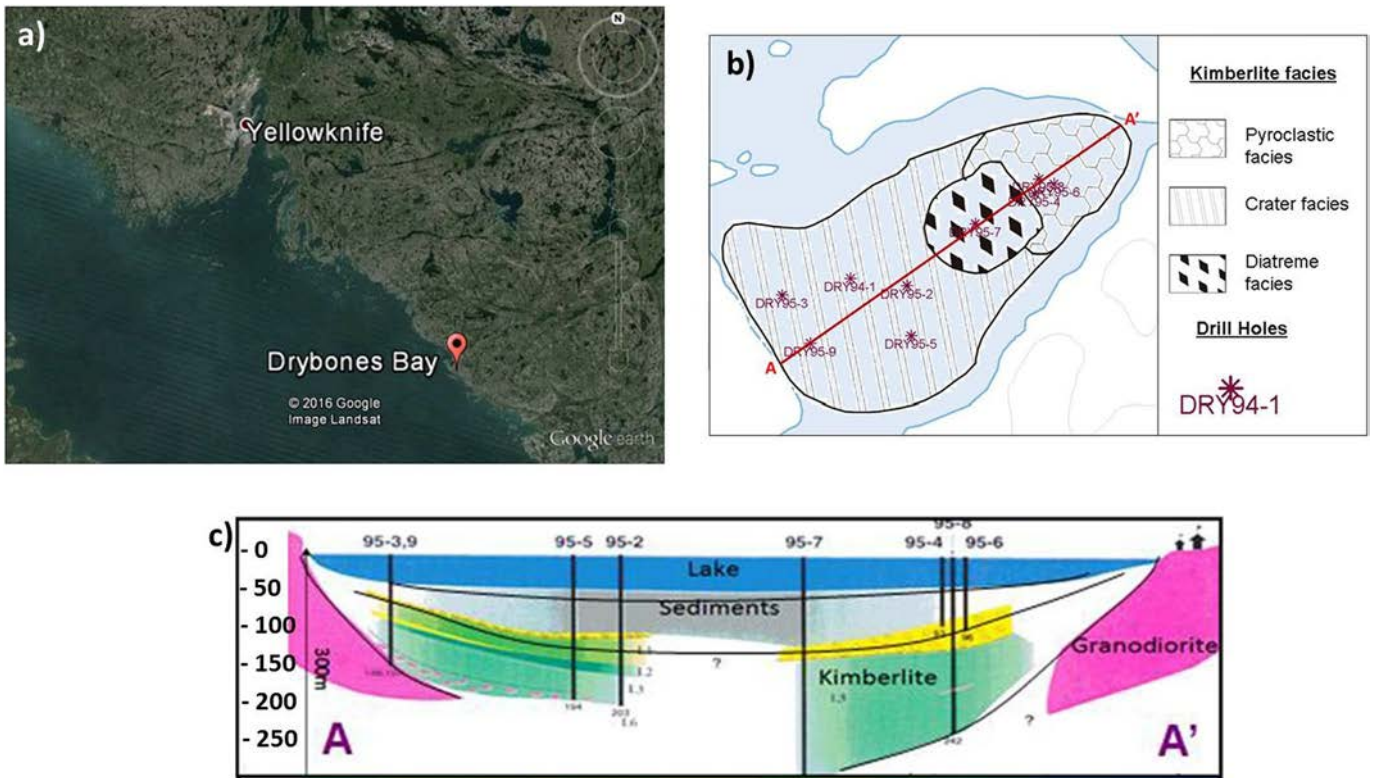
Fig. 6. (a) Geographic location of Drybones bay (Google Earth); (b) Schematic geology of the Drybones pipe below lake sediments and the locations of 1994–95 drilled wells (adapted from Kretchmar, 1995); (c) Geological cross-sections along the profile AA' based on drilling (adapted from Kretchmar, 1995).

depth and a reduction of the investigation depth. We refer to Appendix A for a brief description of the used algorithm.

The following starting model was used for the Cole-Cole inversion: $\rho = 300$ Ohm·m; $m_0 = 100$ mV/V; $\tau = 10^{-3}$ s; $C = 0.5$, where ρ is the resistivity (Ohm·m), m_0 is the chargeability (mV/V), τ is the relaxation time (s) and C is the frequency parameter (dimensionless).

The algorithm converged in 14 iterations with an average misfit of 1.29 (dimensionless, normalized by standard deviation), showing

good overall data fit and so producing a model of electrical resistivity, chargeability, time constant and frequency parameter.

The inversion of VTEM data over Drybones kimberlite, carried out using Cole-Cole model is in better agreement with ZTEM inversions (Kaminski and Oldenburg, 2012, Fig. 8), than the inversion of VTEM data carried out without Cole-Cole modelling.

The comparison between the inversion results and previous inverse models recovered without considering the IP effects in TDEM data
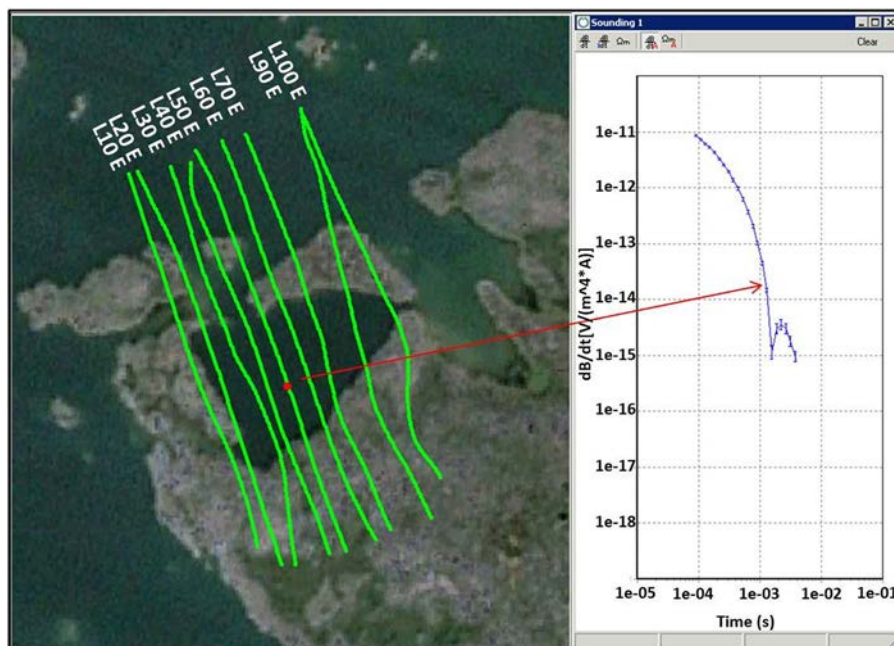

Fig. 7. evidence for IP effects in VTEM data, occurring in correspondence of the kimberlite.
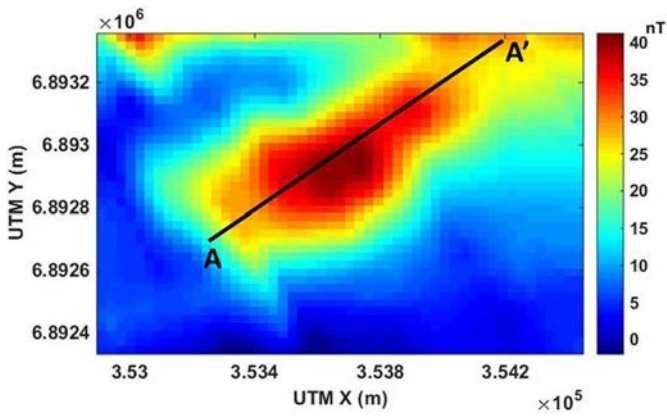
Fig. 8. Total field anomalies above the kimberlite of Drybones bay.

(Kaminski and Oldenburg, 2012, Fig. 6 and Fig. 8), confirmed the importance of modelling the IP effects. Conversely, in our case, where we have modelled the IP effects, retaining the negative voltage data, a significant increase of the recoverability of the resistivity distribution at depth is now achieved.

About magnetic data (Fig. 8), we have performed the inversion of the vertical soundings along the AA' profile located over the kimberlite. Each vertical sounding consists of magnetic data upward continued to 15 different altitudes, from the first level at 170 m above the ground up to the highest level at 240 m above the ground, with a 5 m constant vertical step (Fig. 9a).

For the calculation of the matrix kernel, we have defined a model volume with average horizontal dimensions estimated by the total horizontal derivative method (Cordell and Grauch, 1985). The total horizontal derivative method applied on the magnetic data of Fig. 8 shows complex edges for the magnetic sources (Fig. 9b). The maximum NW and SE estimated dimensions agree with what argued by Kretchmar (1995) for an elongated intrusion of 900 m by 400 m.

The vertical dimension of the model volume is defined to completely contain the source of anomaly by a maximum-depth rule (Fedi and Florio, 2013). In fact, no matter the kind of source distribution, Smith rules (Smith, 1959) or the recent method proposed by (Fedi and Florio, 2013), are very useful in determining the maximum possible depth to the source for a given anomaly.

The volume is then discretized with 100 layers of 10 m thickness to have a satisfactory depth resolution. Susceptibility constraints ($0 \leq j \leq$

10^{-2}) and a constraint on experimental data error ($0 \leq d\mathbf{B} \leq 0.5$ nT) are added to regularize the inversion.

The resistivity, the chargeability and the susceptibility models (Fig. 10) were verified against the known geology along the cross-section AA' (Fig. 6c).

The resistivity section (Fig. 10a) appears rather consistent with the outline of the different layers as determined by wells information. The yellow-red zone reflects the presence of water-saturated fine-grained sediments below the lake water, at the bottom of the bay, with low values of resistivity (< 100 Ωm). Below these formations, a lateral contact is marked between the kimberlite (yellow-green zone below the sediments, with resistivity values in the interval between 100 and 500 Ωm) and granodiorite (high values of resistivity, > 500 Ωm).

Thus, the resistivity section, obtained by modelling airborne IP produces results consistent with the available geological information. A good correlation with the shallowest part of the geological model is found, especially considering that the first time-gate of the system has a central time of 130 μs after the end of ramp, and therefore the near-surface resolution was expected to be limited.

The chargeability section (Fig. 10b) shows a high chargeable layer in correspondence to the lake sediments that, in fact, are expected to be very chargeable for the presence of fine-grained products (clay). The effect of these sediments does not allow an easy detection of the crater facies of the kimberlite that, usually, can produce an IP effect because of weathering, (Macnae, 1979).

The Vertical Soundings inversion of the magnetic data along the AA' profile allows recovering a model with high susceptibilities, possibly associated with the kimberlite body (Fig. 10c). In fact, the estimated depths (top of the kimberlite at about 50 m above sea level) are consistent with the geological information derived by the available drill holes, from which the top of the kimberlite was detected at depth of 100–110 m from the surface. The susceptibility model shows that the magnetized body is clearly separated from the overlying non-magnetic sediments and lake water.

The most magnetized material should mark the shallowest portion of the kimberlite that is subject to geochemical alteration (Kaminski and Oldenburg, 2012). In fact, the mineralogical analysis of the Drybones kimberlite samples revealed signs of alteration due to elevated contents of Cr and Nb, as well as due to low totals of TiO_2 in ilmenites (Dunn et al., 2001). This geochemical alteration may have a strong influence on the magnetic properties of the kimberlite, causing an increase of the magnetization (Dunn et al., 2001).

The comparison between the EM and the magnetic models revealed, in this case, the different sensitivity of the two methods with respect to
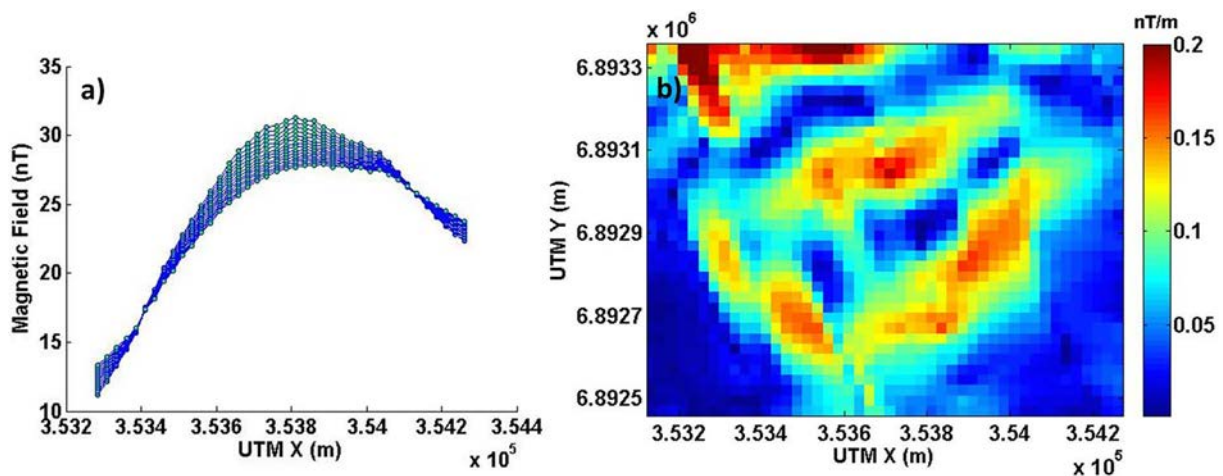

Fig. 9. (a) Behaviour of the magnetic data at different altitudes, along the AA' profile. The green dots represent, for each altitude, the horizontal positions of the data and then the individual vertical soundings; (b) total horizontal derivative of magnetic data above the kimberlite. (For interpretation of the references to colour in this figure legend, the reader is referred to the web version of this article.)
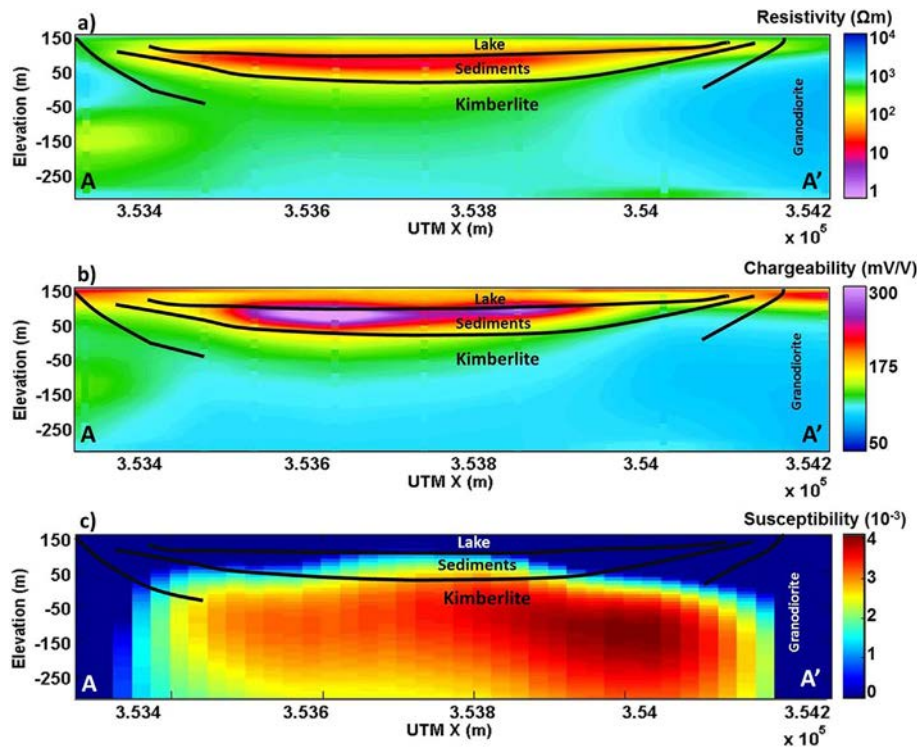
Fig. 10. (a) Resistivity section and (b) chargeability section recovered by SCI inversion using Cole-Cole model along the AA' profile; (c) susceptibility section recovered by Vertical Soundings inversion of aeromagnetic data along the AA' profile.

the investigated geological structures. This allowed a complete characterization of the studied area at Drybones kimberlite but, at same time, it could imply greater difficulty in setting up a true joint inversion, where the physical properties need to be linked in some way by means of petrophysical or empirical relationships (Dell'Aversana, 2014).

4. Conclusions

We showed and discussed the modelling of TDEM and aeromagnetic data related to a helicopter-borne survey flown in 2005 over Drybones Bay, Northwest Territories, Canada, where in 1994 a completely underwater kimberlite structure was discovered.

The evidence of IP effects in the measured EM data, mainly resulting in negative values of the voltage, leaded us using a modified AarhusInv code for their inversion, implementing a Cole-Cole modelling. The presented results suggest a correct hydrogeological interpretation of the cross-section, with lake water and clay-sediment thicknesses supported by drilling results. Clay material appears in our model as conductive and chargeable, while the lake water does not show any chargeable properties. The results presented in this paper appear to be more interpretable and provide better data fit than previous inversion attempts, where the inversion was carried out without considering the IP effects in the TDEM data. The inversions of TDEM data, including the Cole-Cole modelling, can provide an improved recovery of electrical resistivity and chargeability at depth. The extraction of chargeability may be a powerful tool in kimberlite exploration for its key role in mapping crater facies of kimberlites and clay alteration zones, which may be associated with kimberlites.

To better compare the results from magnetic inversion to that of EM data, usually performed on the basis of 1D inversion, the aeromagnetic data were also modelled by a new 1D method allowing the inversion of vertical data soundings. The vertical soundings consisted of magnetic data at different altitudes while the forward problem consisted in assuming a volume of layers of different magnetizations. The volume is finite vertically and horizontally. The inversion of the vertical soundings was performed including inequality constraints on the model

parameters, well reflecting the a-priori knowledge on the studied area. This method presents a reduced computation complexity and even if the algorithm is dealing with a mono-dimensional vertical inversion and the 2D model is built approximating multi-set of 1D models, we obtained a good fitting between the measured and the estimated data along all the profiles.

The integrated study of the results obtained by separately inversion of the TDEM and the aeromagnetic data shows that the two methods have not the same sensitivity with respect to the geological structures in this area. In fact, while the most conductive/chargeable structures are found in correspondence of the water lake and the uppermost lake sediments, the most magnetized structure coincides with the depths to the top of the kimberlite sequence, showing susceptibility values much higher of the poorly-to-not magnetic overlying structures.

Nevertheless, their ability in characterizing sources at different depth ranges of the Drybones Bay, is definitely useful to improve the final interpretation model. All the geological structures at Drybones Bay are well retrieved by the inversion processes and are in very good agreement with the drill hole information available for this area.

Acknowledgements

The authors are highly thankful to Geotech, Ltd. for providing the VTEM data for research purposes.

Appendix A. Laterally constrained inversion for IP parameters

The induced polarization (IP) effects in TDEM data is usually observed in the data derived from coincident-loop systems, showing abnormal fast EM decay with the existence of negative values of the voltage. This phenomenon can significantly alter the shape of the transient and, if not considered, may lead to recover false structure, with incorrect conductivity-thickness parameters (Viezzoli et al., 2015).

Over the years, the handling of the IP effects in TDEM data has kept its relevance with a further interest from ground to airborne data (Smith and Klein, 1996; Kratzer and Macnae, 2012). For airborne data

the appearance of IP effects is closely related to the flight height and to the waveform shape (Viezzoli et al., 2013). The increase of flight height causes a delay in the appearance of the IP effects, which can also disappear if the transition occurs below the noise level. The duration of turn-off controls the injection time of the induced currents in the ground that in turn controls its effective charging. Therefore, a slower turn-off current causes the IP effects to dominate over the induced currents at earlier times.

Viezzoli et al., 2013 have also investigated the dependence of the IP effects in the AEM systems, varying the Cole-Cole parameters and they concluded that the values of resistivity and chargeability are positively correlated with an increase of IP effects, i.e. the IP effects appear at earlier times, while for C and τ they did not observe a similar behavior. The increase of their values is not always followed by an appearance of the IP effects at earlier times.

The possibility of extracting chargeability information from transient EM data, that can have a significant impact to mineral exploration, has provided several suggestions to handle the IP effect with Cole-Cole model.

A polarizable earth may be described using an impedance model derived from the empirical Cole-Cole model (Cole and Cole, 1942):

$$Z(\omega) = \rho \left[1 - \frac{m_0}{10^3} \left(1 - \frac{1}{1 + (i\omega\tau)^C} \right) \right] \tag{A.1}$$

Eq. A.1 introduces a complex impedance relationship, as a function of four parameters: ρ (Ωm) is the electrical resistivity, m_0 (mV/V) is the chargeability, C (dimensionless) is the frequency parameter, describing the variation of phase with frequency and τ (s) is the relaxation time.

Fiandaca et al., 2012) have introduced a 1D algorithm allowing to solve for complex impedance model; here the Cole-Cole model (eq. A.1) represents the forward mapping kernel. The four Cole-Cole parameters are the unknowns of the inverse problem which are simultaneously obtained in a unique inversion process, where the relationship between parameters is maintained at all times. The inversion has been implemented using the 1D laterally constrained inversion (LCI) scheme (Auken et al., 2005): a set of vertical and lateral constraints, tied together the parameters of the neighboring soundings along the flight lines for LCI, retrieving 2D sections in quasi-layered environments (Fig. A.1).
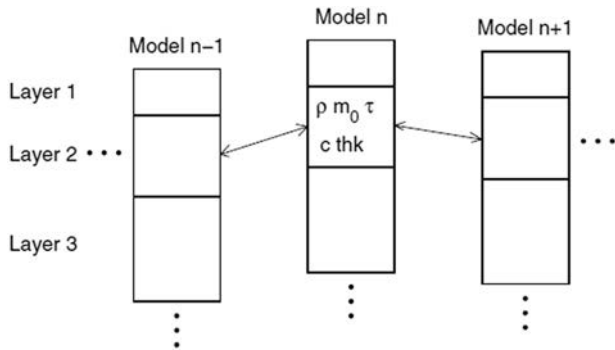

Fig. A.1. Model parameters with lateral constraints (adapted from Fiandaca et al., 2012).

The LCI inversion algorithm is described in detail in Auken and Christiansen (2004). It allows performing the inversion of large data set, where the parameters of the earth model for each sounding are connected laterally by means of lateral constraints, defining a specified variance of the model parameters. The lateral constraints can be considered as a-priori information on the geological variability in the area of measurements. In LCI, the connection of the soundings occurs along a profile, producing quasi-2D images of the subsurface with smooth lateral transitions. The constraints allow the migration of information from one model to neighboring models, helping to resolve areas with poorly constrained parameters or soundings particularly noisy.

The LCI is a full non-linear damped least squares inversion based on an exact forward solution, modelling the instrumentation's system transfer function (STF). The solutions developed by Ward and Hohmann (1988) are used as the basis for the forward modelling algorithm. Modelling the STF also includes low-pass filters (Effersø et al., 1999), and turn-on/turn-off ramps (Fitterman and Anderson, 1987).

The inversion problem can be written:.

$$\begin{bmatrix} \mathbf{G} \\ \mathbf{R} \end{bmatrix} \mathbf{dm_{true}} = \begin{bmatrix} \mathbf{D_{obs}} \\ \mathbf{dr} \end{bmatrix} + \begin{bmatrix} \mathbf{e_{obs}} \\ \mathbf{e_r} \end{bmatrix} \tag{A.2}$$

where dDobs denotes the observed data, eobs is the error on the observed data, G is the Jacobian and contains all partial derivatives of the mapping, dr are the constraints, er is the error on the constraints with 0 as expected value and R is the roughening matrix, containing 1's and − 1's for the constrained parameters, and 0 in all other places.

The covariance matrix for the joint observation error, which it is assumed to be a diagonal matrix, becomes:.

$$\mathbf{C}' = \begin{bmatrix} \mathbf{C_{obs}} & 0 \\ 0 & \mathbf{C_R} \end{bmatrix} \tag{A.3}$$

if any a-priori information on model parameters, allowing to reduce the ambiguity on the inverse models, are available, they can be added, following Jackson (1979), as an extra row ($\mathbf{m_{prior}}$) to the system A.2 and the a-priori model variance ($\mathbf{C_{prior}}$) is described in covariance matrix.

In a compact form, Eq. A.2 is rewritten as:.

$$\mathbf{G}'\mathbf{dm_{true}} = \mathbf{dD}' + \mathbf{e}' \tag{A.4}$$

the model estimate is (Menke, 1984):

$$\mathbf{dm_{est}} = \left(\mathbf{G}'^{\mathbf{T}}\mathbf{C}'^{-1}\mathbf{G}' \right)^{-1} \mathbf{G}'^{\mathbf{T}}\mathbf{C}'^{-1}\mathbf{dD}' \tag{A.5}$$

that minimizes the objective function:

$$\mathbf{Q} = \left(\frac{1}{\mathbf{N} + \mathbf{A}} \left[\mathbf{dD}'^{\mathbf{T}}\mathbf{C}'^{-1}\mathbf{dD}' \right] \right)^{\frac{1}{2}} \tag{A.6}$$

The algorithm inverts all the soundings simultaneously, considering all the data and the lateral constraints. A common objective function is thus minimized. The output model, including all the 1D soundings, is balanced between the constraints, the physics and the data.

Following this approach, some experiments on synthetic AEM data were presented by Viezzoli et al. (2013), showing how 1D inversion is able to recover the unknown parameters and which is their standard deviation, for a chargeable half-space. These tests have highlighted that, in general, the resistivity and chargeability parameters are well-resolved, displaying also some degree of coupling. Low standard deviations are usually associated to the frequency parameter C, for which a low value of starting model is preferable to obtain better convergence and sensitivity. τ parameter is the worst resolved and in addition it has been noted that a starting value close to real value is needed to avoid a negative influence on all the other parameters.

References

Auken, E., Christiansen, A.V., 2004. Layered and laterally constrained 2D inversion of resistivity data. Geophysics 69, 752–761.

Auken, E., Christiansen, A.V., Jacobsen, B.H., Foged, N., Sørensen, K.I., 2005. Piecewise 1D laterally constrained inversion of resistivity data. Geophys. Prospect. 53, 497–506.

Baranov, W., 1975. Potential Fields and their Transformations in Applied Geophysics. Gebruder Borntraeger, Berlin.

Blakely, R.J., 1996. Potential Theory in Gravity and Magnetic Applications. Cambridge University Press, Cambridge.

Bowring, S.A., Housch, T., 1995. The Earth's early evolution. Science 269, 1535–1540.

Castaldo, R., Fedi, M., Florio, G., 2014. Multiscale estimation of excess mass from gravity data. Geophys. J. Int. 197, 1387–1398.

Cole, K.S., Cole, R.H., 1942. Dispersion and absorption in dielectrics. J. Chem. Phys. 9-4, 341–351.

Cordell, L., Grauch, V.J.S., 1985. Mapping basement magnetization zones from aeromagnetic data in the San Juan basin. In: Hinze, W.J. (Ed.), The Utility of Regional Gravity and Magnetic Anomaly Maps. Society of Exploration Geophysicists, New Mexico, pp. 181–197.

Dell'Aversana, P., 2014. Integrated Geophysical Models. EAGE Publications bv, HOUTEN The Netherlands.

Dunn, C.E., Smith, D., Kerr, D.E., 2001. Biogeochemical survey of the Drybones Bay area. NWT using outer bark of black spruce. Geological Survey of Canada, Open File. 3919.

Effersø, F., Auken, E., Sørensen, K.I., 1999. Inversion of band-limited TEM responses. Geophys. Prospect. 47, 551–564.

Fedi, M., Florio, G., 2013. Determination of the maximum-depth to potential field sources by a maximum structural index method. J. Appl. Geophys. 88, 154–160.

Fedi, M., Rapolla, A., 1995. Vertical Gravity an Magnetic Soundings: forward problem formulation and data inversion. Boll. Geofis. Teor. Appl. Vol. XXXVII, N.147.

Fiandaca, G., Auken, E., Christiansen, A.V., Gazoty, A., 2012. Time-domain induced polarization: full-decay forward modelling and 1D laterally constrained inversion of Cole-Cole parameters. Geophysics 77, E213–E225.

Fitterman, D.V., Anderson, W.L., 1987. Effect of transmitter turn-off time on transient soundings. Geoexpl. 24, 131–146.

Haggerty, S.E., 1986. Diamond genesis in a multiply-constrained model. Nature, Volume 320, 34–38.

Jackson, D.D., 1979. The use of a priori information to resolve non-uniqueness in linear inversion. Geophys. J. R. Astron. Soc. 57, 137–157.

Janse, A.J.A., 1993. The Aims and Economic Parameters of Diamond Exploration. Diamonds, Exploration, Sampling and Evaluation, Prospectors and Developers Association of Canada, pp. 173–184.

Kaminski, V., Oldenburg, D., 2012. The geophysical study of Drybones kimberlite using 3D time domain EM inversion and 3D ZTEM inversion algorithms: 22nd ASEG Geophysical Conference and Exhibition, Extended Abstracts. pp. 1–4.

Kaminski, V., Legault, J.M., Kumar, H., 2010. The Drybones kimberlite: a case study of VTEM and ZTEM airborne EM results, 21ST ASEG International Geophysical Conference and Exhibition, Extended Abstract (22-25 August 2010, 4 ppSydney, Australia).

Kjarsgaard, B.A., 1996. Kimberlites. In: LeCheminant, A.N., Richardson, D.G., DiLabio, R.N. W., Richardson, K.A. (Eds.), Searching for Diamonds in Canada. 3228. Geological Survey of Canada, Open File, pp. 29–37.

Kratzer, T., Macnae, J., 2012. Induced polarization in airborne EM. Geophysics 77 (5), E317–E327.

Kretchmar, U., 1995. Drill Report on the Drybones Bay Kimberlite Property. Drybones Bay, Great Slave Lake, District of MacKenzie, Northwest Territories, Canada.

Lane, R., Brodie, R., Fitzpatrick, A., 2004. Constrained inversion of AEM data from the lower Balonne area, southern Queensland, Australia. Lower Balonne airborne geophysical project. CRC LEME OPEN FILE REPORT 163.

Le Cheminant, A.N., van Breemen, O., 1994. U-Pb ages of Proterozoic dyke swarms, lac de Gras area, N.W.T.: evidence for progressive break-up of an Archean supercontinent. GAC Programs with Abstracts 19, p. 62.

Le Cheminant, A.N., Heaman, L.M., van Breemen, O., Ernst, R.E., Baragar, W.R.A., Buchan, K. L., 1996. Mafic magmatism, mantle roots, and kimberlites in the slave craton. In: Le Cheminant, A.N., Richardson, D.G., DiLabio, R.N.W., Richardson, K.A. (Eds.), Searching for Diamonds in Canada. 3228. Geological Survey of Canada, Open File, pp. 161–169.

Macnae, J.C., 1979. Kimberlites and exploration geophysics. Geophysics 44 (8), 1395–1416.

Menke, W., 1984. Geophysical data analysis, discrete inverse theory. 260. Academic Press.

Menke, W., 1989. Geophysical data analysis: Discrete inverse theory. Academic Press (Elsevier).

Pell, J.A., 1995. Kimberlites in the Slave Structural Province. Northwest Territories: A Preliminary Review. EGS 1995–12. NWT Geological Mapping, Indian and Northern Affairs Canada (20 pages).

Power, M., Hildes, D., 2007. Geophysical strategies for kimberlite exploration in northern Canada. Geophysical case histories. In: Milkereit, B. (Ed.), Paper 89. Proceedings of Exploration 07: Fifth Decennial International Conference on Mineral Exploration, pp. 1025–1031.

Reed, L.E., Witherly, K.E., 2007. 50 years of kimberlite geophysics, a review. In: Milkereit, B. (Ed.), Proceedings of Exploration 07: Fifth Decennial International Conference on Mineral Exploration, pp. p679–p689.

Scott Smith, B.H., 1996. Kimberlites. In: Mitchell, R.H. (Ed.), Undersaturated Alkaline Rocks: Mineralogy, Petrogenesis and Economic Potential. Vol. 24. Mineralogical Association of Canada, Short Course Volume, pp. 217–244.

Smith, R.A., 1959. Some depth formulae for local magnetic and gravity anomalies. Geophys. Prospect. 7, 55–63.

Smith, R.S., Klein, J., 1996. A special circumstance of airborne induced polarization measurements. Geophysics 61, 66–73.

Viezzoli, A., Christiansen, A.V., Auken, E., Sørensen, K., 2008. Quasi-3D modeling of airborne TEM data by spatially constrained inversion. Geophysics 73, 105–113.

Viezzoli, A., Fiandaca, G., Segio, S., Auken., E., 2013, Constrained Inversion of IP Parameters from Airborne EM Data , ASEG-PESA Expanded abstracts, Melbourne, Australia.

Viezzoli, A., Kaminski, V., Cooper, Y.L., Hardy, L., Fiandaca, G., 2015. Improving Modelling of AEM Data Affected by IP, Two Case Studies. ASEG-PESA Expanded abstracts, Perth, Australia.

Vitale, A., Fedi, M., Di Massa, D., Florio, G., 2016. A New Algorithm for Inversion of 1D Vertical Soundings of Potential Field Anomalies. 78th EAGE Conference & Exhibition 2016 Wien (Austria).

Ward, S.H., Hohmann, G.W., 1988. Electromagnetic theory for geophysical applications. In: Nabighian, M.N. (Ed.), Electromagnetic methods in applied geophysics: SEG. 131–311.

Witherly, K., Irvine, R., Morrison, E., 2004. The Geotech VTEM Time Domain helicopter EM System, In Expanded Abstract of 74th Ann. International meeting SEG, Denver. pp. 1217–1220 (Colorado (USA)).